ARTICLES

NMR Relaxation Studies of the $^{13}CH_3$ Spin Grouping in the Vicinity of the T_1 Minimum

Marie-Thérèse Chenon,*,† Reinhard Dunkel,‡ David M. Grant,§ and Lawrence G. Werbelow||

LADIR, CNRS, 2 Rue Henry Dunant, 94320 Thiais, France, ScienceSoft Corporation, 470 S. 1300 E. #1004, Salt Lake City, Utah 84102, Department of Chemistry, University of Utah, Salt Lake City, Utah 84112, and Department of Chemistry, NMIMT, Socorro, New Mexico 87801

Received: June 9, 1998; In Final Form: September 18, 1998

The perturbation-response behavior of various nuclear spin polarizations associated with methanol's $^{13}CH_3$ spin grouping were examined in the vicinity of the T_1 minimum. Dipole−dipole auto- and cross-correlation spectral densities indicate unhindered methyl rotation about a triad axis oriented perpendicular to the principal axis of an axially symmetric reorienting molecular framework. This finding is consistent with a strongly associated solute (methanol)/solvent (glycerol) mixture. In the motional regime investigated, it is predicted that relaxation-induced polarization transfer is manifest in differential frequency shifts of various multiplet components. Indeed, this study clearly demonstrates reproducible second order spectral shifts. However, the theory developed in this work accounts for only a portion of the observed shifts.

I. Introduction

Increasingly, NMR is being used to elucidate both solution-state structures[1] and motions[2] of large molecules. As multidimensional NMR methods manipulate the spin systems so as to populate multiquantum coherences other than the traditional single-quantum coherences, a better understanding of relaxation-induced polarization transfer (RIPT) becomes important to structural methods. In addition, the study of RIPT has the ability to provide important details on the local mobility of molecular moieties containing several magnetically coupled nuclei, among which ^1H and ^{13}C are the most familiar. For example, a RIPT analysis of a continuous hydrocarbon chain yields information on the motion of the carbon backbone,[3] while the methyl group in methanol dissolved in glycerol may be used to simulate the motional model of methyl groups in biomolecules such as proteins. Conveniently, the viscosity dependence of glycerol over ambient temperatures simulates the dynamics of such macromolecules for relaxation processes in the interesting T_1 minimum region found just beyond the extreme narrowing limit. Hence, RIPT principals[4−7] obtain, and the Redfield method[8] can be used to characterize the relaxation.

Biomolecular dynamics usually fall outside the extreme narrowing limits, and only a few RIPT papers are available in this motional regime.[9,10] For such molecules, quantitative descriptions of the relaxation process become more complex and certain features are uncommonly sensitive to cross-correlation spectral densities. In addition, relaxation in the vicinity of the T_1 minimum, where extreme narrowing begins to fail, can induce dynamic frequency shifts.[11,12] The dynamic frequency shift may be ignored only if cross-correlation is absent or extreme narrowing obtains.

Many papers have dealt with dynamic frequency shifts for quadrupolar nuclei and, more recently, for spin-1/2 nuclei coupled to nuclei with spins greater than 1/2.[13−17] Very recently,[11,18−20] there has been a growing interest in dynamic frequency shifts for spin systems with only spin-1/2 nuclei. There is some evidence in the literature that effects attributed to the dynamic frequency shift were seen in published methyl proton inversion−recovery spectra recorded many years ago.[21−23] At that time, it was argued by Werbelow et al.[20,24] that proton dipole−dipole cross-correlation could remove the spectral degeneracy resulting in a multiplet structure of the proton resonance.

In this paper, the dynamics of methanol in glycerol is deduced from various dipole−dipole spectral densities. Also, we present direct experimental evidence of the existence of different frequencies for the components of the central lines of the methyl quartet. A preliminary communication of these data has appeared elsewhere.[25]

II. Experimental Section

The samples used in this study were 0.85 M solutions of $^{13}CH_3OD$ in glycerol-d_8. The enrichment levels of ^{13}C and ^2H (D) were 99% and 98% respectively. Care had to be taken to keep the ^{18}O isotope at the natural abundance level since an initial sample exhibited an isotopic effect induced by a significant amount of ^{18}O generated during the ^{13}C enrichment process. Glycerol-d_8 was uniformly deuterated at 98%. Both compounds were purchased at Isotec (USA). Dissolved oxygen was removed by three successive freeze−pump−thaw cycles, then the solution was rapidly transferred under an argon atmosphere into two NMR sample tubes for studying at 9.4 and 11.7 T. An acetone-d_6 sample sealed in a capillary tube was

* To whom correspondence should be addressed. Fax: 33 1 49 78 13 23. E-mail: chenon@glvt-cnrs.fr.
† LADIR.
‡ ScienceSoft Corporation.
§ University of Utah.
|| NMIMT.

10.1021/jp982564j CCC: $18.00
Published on Web 03/03/1999

inserted into the 9.4 T sample and used as a field lock. Both samples were closed with screw caps and sealed with Teflon tape. The height of the solution in the NMR sample tube was selected to achieve good magnetic field homogeneity while minimizing the diffusion of the spins in and out of the receiver coil. The carbon signals, found 0.142 ppm at higher frequency from those of $^{13}CH_3OD$, account for the small but still measurable amount of $^{13}CH_3OH$ in the sample.

Decoupled (CW) carbon inversion−recovery experiments were run from 50 °C down to −30 °C on a Varian XL-400 spectrometer as well as carbon inversion−recovery (CIR) experiments at 35, 5, and −20 °C. This latter set of temperatures was also used for the coupled relaxation experiments performed on a Varian VXR-500 spectrometer. The response characteristics of the carbon magnetization were observed after different perturbations of either the proton or carbon magnetization (inversion−recovery, hard pulse, soft pulse, *J*-pulse[26]). Furthermore, a CIR experiment was done at −10 °C. The various proton and carbon pulse lengths were calibrated before each experiment. It was necessary to use a very long recycle time, at least 30 times the nominal T_1, to ensure that all forms of multispin order were thermalized.

Given the small magnitude of the effects observed, every effort was made to eliminate all potential sources of error. The data were acquired in blocks of four or eight transients, and the data acquisition was cycled through all the evolution times (d2) listed randomly in order to minimize the effects of the spectrometer drift. Furthermore, every third to fifth block was used to record the equilibrium magnetization. Each of the four peaks of the ^{13}C quartet was normalized, independently, by comparison with its thermal equilibrium value.

III. Data Processing Details

The program 1D_ANALYSIS[27,28] was written to characterize the strongly overlapping signals in the CH_3OD in glycerol-d_6 relaxation data. On the basis of the 1D_ANALYSIS program, LOCKIT was implemented for observe-channel software locking of the data acquisition without polluting the sample with lock substances.

Spectral Analysis Software: 1D_ANALYSIS. This program is part of a software package for analyzing multidimensional phase-sensitive experimental data using a nonlinear regression fitting algorithm.[29−31] The approach starts with a simple peak-picking step in order to identify the spectral regions of interest. It then progresses to the regression analysis of individual spectral resonances. The final step is regressing complete groups of overlapping resonances. The two initial steps may be skipped by providing a list of spectral resonances. The 1D_ANALYSIS program optimizes all parameters that are not locked to predetermined values.

The regression model, used by 1D_ANALYSIS, consists of a sum of complex-valued overlapping resonances in the frequency domain. Each component resonance is modeled as the convolution of a Lorentzian line shape resulting from spin relaxation and a sinc line shape resulting from the finite FID acquisition period. Each component resonance is characterized by four independent parameters: the integrated signal intensity, the resonance frequency, the effective relaxation time T_2* (inversely related to the signal width at half-height), and the signal's phase angle. The acquisition time is known from the experimental setup. Through the multistep regression analysis, the program can determine an accurate numerical signal description, even for overlapping resonances. The description can be used to selectively remove spectral resonances from the spectrum (e.g., for solvent suppression), to accurately auto phase the spectrum,[32] and to deconvolute overlapping signal regions.

Locking Data Acquisition through Software LOCKIT. The internal deuterium field-frequency lock circuit, used to compensate for the magnet drift, avoids the broadening of resonances during long-term data acquisitions. However, a wide range of experiments are not feasible using this hardware lock. For example: (1) the deuterium lock has to be switched off when observing deuterium, (2) the deuterium lock channel is used for broadband deuterium decoupling (e.g., perdeuterated proteins);[33−36] (3) in-vivo and localized spectroscopy samples cannot be enriched in deuterium; (4) capillary[37] or nano samples[38] are too volume limited to obtain a stable lock through adding deuterium lock substances. For this study, the high viscosity of CH_3OD in glycerol-d_6 resulted in deuterium resonances of the sample too broad for high-precision locking. Addition of a lock substance to the sample would have decreased the sample viscosity, hence limiting the study to the extreme narrowing domain. A capillary tube, filled with a lock compound, gave satisfactory results on the Varian XL-400 but resulted in unacceptable homogeneity problems on the Varian VXR-500.

Internal homonuclear locks provide a flexible solution for these field stability problems, and internal lock circuits have been used extensively with TMS in continuous-wave proton spectrometers.[39] With the LOCKIT software, developed by Dunkel,[40] one acquires a number of transients in small blocks and these are designated as FID components. The number of transients per block is chosen to be as small as possible in order to minimize the residual drift of the magnetic field during the acquisition of each FID component. After each component acquisition, the drift of one or more of the resonance frequencies in the spectrum is monitored. By analogy with a hardware lock, LOCKIT is given direct control of the magnetic field strength by using z_0 shim adjustments. Due to its function for locking and shimming, the z_0 shim is normally under computer control and frequently has a sufficient resolution for this application. For the older Varian VXR-500 spectrometer, the z_0 resolution had to be increased by adding a switchable resistor between the shim DAC and the probe (resolution enhancement 40 times to 0.027 Hz per z_0 step at 500 MHz). On newer NMR instruments, especially when observing or locking on deuterium, the standard z_0 resolution is often sufficient for the use of LOCKIT.

For this study, the minimum number of phase-cycling transients (either four or eight depending upon the pulse sequence) was acquired in one uninterrupted FID component. These components were taken in an interleaved fashion to average any nonrandom changes in the spectrometer during the overnight set of acquisitions. For each FID component, 1D_ANALYSIS was used to determine the true resonance frequencies of the outer resonances, A and D, of the carbon quartet. The required lock correction was then calculated from these frequencies. Due to different relaxation times, both transitions are unlikely to go simultaneously through zero intensity in any given spectrum. Both resonances depend on temperature, but in each separate experiment they were assumed to be constant in frequency for the various evolution times used. When the resonance frequencies were sufficiently accurate, a FID component was combined with previously acquired transients. Otherwise, the magnetic field was adjusted further and the FID component reacquired. LOCKIT always out performed the 10% field-frequency stability of the smallest line width found in a given experiment; this level of accuracy was deemed adequate for this study.

In summary, the LOCKIT software is an effective lock mechanism that can be used on standard NMR equipment usually without hardware modifications. The repetition frequency for correcting drift is limited by the data acquisition rate, but most NMR magnets are sufficiently stable for this repetition rate to avoid noticeable broadening of the resonances. LOCKIT can be applied to either the observe or lock channels and operate during the acquisition cycle of a deuterium spectrum. This software eliminates the need for fluorine lock probes and hardware extensions. With LOCKIT, deuterium decoupling is possible and sample pollution with additional lock compounds is avoided. The approach may also be used on solid-state or imaging equipment that commonly lacks field-frequency lock hardware.

IV. Theoretical Section

Much of the necessary theoretical framework for analysis of the perturbation-response characteristics of the $^{13}CH_3$ spin grouping has been described in detail elsewhere.[4,5,41] In this section, a few of the relevant aspects utilized in this study are summarized.

Assuming spatial isotropy, the evolution of any one of the five independent observable polarizations, in general, can be represented by a weighted sum of 11 exponentials.[42] If extreme narrowing obtains or certain interactions are absent, simpler descriptions may result. After a specific perturbation, individual relaxation rates may be deduced from a least-squares fit of the resulting relaxation curves. Linear combinations of a sufficient number of these specific rates ultimately will yield individual spectral densities. As a final step, interpretation of the spectral densities in terms of interaction strength and dynamic parameters depends on a chosen motional model. Alternatively, as demonstrated in this study, this analysis may be simplified by recognizing that certain relaxation rates are identified with individual spectral densities.

Following the notation and numbering scheme introduced earlier,[4] the observables and associated operator equivalents for this system are defined as follows: ${}^a\nu_1 = \langle \Delta I_z \rangle$ is proportional to the sum of the deviations in intensity from thermal equilibrium of the four lines of the ^{13}C quartet; ${}^a\nu_2 = (1/\sqrt{3})\langle \Delta(S_z + S_z' + S_z'') \rangle$ is proportional to the summed deviation intensity of the ^1H (i.e., S spin) doublet; ${}^a\nu_3 = (4/\sqrt{3})\langle I_z(S_zS_z' + S_zS_z'' + S_z'S_z'') \rangle$ is proportional to 3 times the intensity of the outermost lines minus the innermost lines in the ^{13}C quartet; ${}^s\nu_1 = (2/\sqrt{3})\langle I_z(S_z + S_z' + S_z'') \rangle$ is proportional to 3 times the intensity difference of the outermost lines plus the intensity difference of the innermost lines in the ^{13}C quartet; ${}^s\nu_2 = 8\langle I_zS_zS_z'S_z'' \rangle$ is proportional to the intensity difference of the outermost lines minus the intensity difference of the innermost lines in the ^{13}C quartet.

As suggested above, certain relaxation rates can be identified with individual spectral densities. If the following interactions are responsible for nuclear spin relaxation in $^{13}CH_3$, mutual dipole−dipole (D_{CH}, $D_{HH'}$), electronic shielding anisotropy (SA_H, SA_C), and random field (R_C, R_H) interactions (e.g., spin-rotation, paramagnetic impurities), it is easily shown that the rate of polarization transfer between ${}^a\nu_1$ and ${}^a\nu_3$ is given by $(2\sqrt{3})K^{D_{CH}D_{CH'}}(\omega_C)$, the rate of polarization transfer between ${}^a\nu_2$ and ${}^a\nu_3$ is given by $4K^{D_{CH}D_{HH'}}(\omega_H)$, and the rate of polarization transfer between ${}^a\nu_1$ and ${}^s\nu_1$ is given by $-(4\sqrt{3})K^{D_{CH}SA_C}(\omega_C)$. Almost as simple are the rate of polarization transfer between ${}^a\nu_2$ and ${}^s\nu_1$, which is given by $-(4/9)\{7K^{D_{CH}SA_H}(\omega_H) + 2K^{D_{CH}SA_{H'}}(\omega_H)\}$, and the rate of polarization transfer between ${}^s\nu_1$ and ${}^s\nu_2$, which is given by $(2\sqrt{3})\{K^{D_{CH}D_{CH'}}(\omega_C) + K^{D_{CH}D_{HH'}}(\omega_H)\}$. All of these polarization transfers are induced by cross-correlation or interference effects.

In addition to these polarization transfer rates, any spin relaxation study must consider the information embodied in the conventional self-relaxation rates associated with ${}^a\nu_1$ and ${}^a\nu_2$ which are defined, respectively, as

$$1/T_1({}^a\nu_1) = J^{D_{CH}}(\omega_C - \omega_H) + 3J^{D_{CH}}(\omega_C) + 6J^{D_{CH}}(\omega_C + \omega_H) + 4J^{SA_C}(\omega_C) + R_1{}^C \quad (1a)$$

and

$$1/T_1({}^a\nu_2) = (1/3)J^{D_{CH}}(\omega_C - \omega_H) + J^{D_{CH}}(\omega_H) + 2J^{D_{CH}}(\omega_C + \omega_H) + 2J^{D_{HH'}}(\omega_H) + 8J^{D_{HH'}}(2\omega_H) + 4J^{SA_H}(\omega_H) + R_1{}^H \quad (1b)$$

and the cross-relaxation rate between ${}^a\nu_1$ and ${}^a\nu_2$, which is given by

$$(1/\sqrt{3})\{6J^{D_{CH}}(\omega_C + \omega_H) - J^{D_{CH}}(\omega_C - \omega_H)\} \quad (1c)$$

$R_1{}^C$ and $R_1{}^H$ are assumed to be effective composite random-field contributions.

The following autocorrelation, J^η, or cross-correlation, $K^{\eta\eta'}$, spectral densities ($\eta,\eta' = SA_C$, SA_H, D_{CH}, $D_{HH'}$) have been introduced in the preceding equations:

$$J^{D_{ij}}(\omega) = (3/10)(\mu_o/4\pi)^2(\gamma_i\gamma_j\hbar\langle r_{ij}{}^{-3}\rangle)^2 \,\mathrm{Re}\, G^{D_{ij}D_{ij}}(\omega) \quad (2a)$$

$$J^{SA_i}(\omega) = (1/30)(\Delta\sigma_i\omega_i)^2 \,\mathrm{Re}\, G^{SA_iSA_i}(\omega) \quad (2b)$$

$$K^{D_{ij}D_{ik}}(\omega) = (3/10)(\mu_o/4\pi)^2(\gamma_i{}^2\gamma_j\gamma_k\hbar^2\langle r_{ij}{}^{-3}\rangle\langle r_{ik}{}^{-3}\rangle) \,\mathrm{Re}\, G^{D_{ij}D_{ik}}(\omega) \quad (2c)$$

$$K^{D_{ij}SA_k}(\omega) = (1/10)(\mu_o/4\pi)(\gamma_i\gamma_j\hbar\langle r_{ij}{}^{-3}\rangle)(\Delta\sigma_k\omega_k) \,\mathrm{Re}\, G^{D_{ij}SA_k}(\omega) \quad (2d)$$

The reduced correlation function, $G^{\eta\eta'}(\omega)$, is defined as

$$G^{\eta\eta'}(\omega) = (1/5)\int_0^\infty \langle (P_2(\cos\Theta_\eta(t-\tau)))(P_2(\cos\Theta_{\eta'}(t))) \rangle \times \exp(-i\omega\tau)\,d\tau \quad (3)$$

Re signifies the "real part", and $P_2(\cos\Theta_{\eta'}(t)) = (3\cos^2\Theta_{\eta'}(t) - 1)/2$. The angular arguments, Θ_η, position the principal axes of interaction in the laboratory frame. This orientation is rendered time dependent by molecular movement. It is assumed that the shielding tensor is axially symmetric (see Discussion).

Molecular information can also be obtained from relaxation studies of single- and multiple-quantum coherences. Unfortunately, the accurate measurement of these relaxation rates is often difficult. However, in our study, one aspect associated with the relaxation of coherence, the dynamic frequency shift,[11] is considered. For the ^{13}C quartet, it can be shown (see Appendix) that the frequency separation (in Hz) between the highest frequency and lowest frequency components is $3J_{CH} + \Delta(\delta\nu)$, where

$$\Delta(\delta\nu) = 12\{Q^{D_{CH}SA_C}(\omega_C) + Q^{D_{CH}SA_H}(\omega_H)\}/2\pi \quad (4)$$

J_{CH} is the familiar C−H scalar coupling constant, and

$$Q^{D_{ij}\mathrm{SA}_k} = (1/10)(\mu_o/4\pi)\,(\gamma_i\gamma_j\hbar\langle r_{ij}^{-3}\rangle)(\Delta\sigma_k\omega_k)\ \mathrm{Im}\ G^{D_{ij}\mathrm{SA}_k}(\omega) \quad (5)$$

The dynamic frequency shift is related to the imaginary (Im) component of the reduced correlation function, $G^{\eta\eta'}(\omega)$.

Similarly, the dynamic frequency shift removes the spectral degeneracy between the proton quartet and doublet componentsto the two central members of the ^{13}C quartet. This splitting equals

$$\Delta(\delta\nu) = \{Q^{D_{\mathrm{CH}}D_{\mathrm{CH}'}}(\omega_\mathrm{C} - \omega_\mathrm{H}) - 6Q^{D_{\mathrm{CH}}D_{\mathrm{HH}'}}(\omega_\mathrm{H}) + 6Q^{D_{\mathrm{CH}}D_{\mathrm{CH}'}}(\omega_\mathrm{C} + \omega_\mathrm{H})\}/2\pi \quad (6)$$

where

$$Q^{D_{ij}D_{ik}} = (3/10)(\mu_o/4\pi)^2(\gamma_i^2\gamma_j\gamma_k\hbar^2\langle r_{ij}^{-3}\rangle\langle r_{ik}^{-3}\rangle)\ \mathrm{Im}\ G^{D_{ij}D_{ik}}(\omega) \quad (7)$$

Additional spectral densities (both Re and Im) are important for other features of relaxation in the CH_3 spin grouping. However, these are irrelevant for our study.

Finally, we must introduce the interpretational basis of the correlation functions that play a central role in the penultimate analysis of spin relaxation data. For reasons to be explained more fully in the Discussion, the simplest model that fits the data assumes that the methyl group is attached to a molecular framework which undergoes symmetric toplike reorientation characterized by the diffusion constants $D_{||}$ and $D_\perp$. The methyl group itself undergoes further internal rotation about its triad axis, characterized by the rotational diffusion constant D_i. The angle between the triad axis and the principal motional axis ($D_{||}$) of molecular diffusion is defined by the angle β. The polar angles, θ and ϕ, position the principal axis of the (axially symmetric, rank-two) interaction with respect to the internal rotational axis.

In this model, the Re and Im parts of $G^{\eta\eta'}(\omega)$ are defined as[43,44]

$$\mathrm{Re}\ G^{\eta\eta'}(\omega) = \sum_{n,k} d_{nk}^{\ 2}(\beta)d_{0k}(\theta_\eta)d_{0k}(\theta_{\eta'})\cos(k(\phi_\eta - \phi_{\eta'}))\times \{\tau_{2nk}/(1 + (\omega\tau_{2nk})^2)\} \quad (8a)$$

$$\mathrm{Im}\ G^{\eta\eta'}(\omega) = \sum_{n,k} d_{nk}^{\ 2}(\beta)d_{0k}(\theta_\eta)d_{0k}(\theta_{\eta'})\cos(k(\phi_\eta - \phi_{\eta'}))\times \{\omega\tau_{2nk}^{\ 2}/(1 + (\omega\tau_{2nk})^2)\} \quad (8b)$$

where $1/\tau_{2nk} = 6D_\perp + n^2(D_{||} - D_\perp) + k^2D_\mathrm{i}$ and $d_{nk}(\beta)$ are elements of reduced, second rank, Wigner matrixes.[45] These expressions imply that the internal motion and the overall molecular motion are independent. This usual assumption is supported by a recent femtosecond fluorescence study on the dynamics of deuterated methanols.[46]

The expanded forms of eqs 8 are exceedingly cumbersome. For example, if standard tetrahedral geometry is assumed, the simple autocorrelation function $J^{D_{\mathrm{CH}}}(\omega)$ is defined as

$$J^{D_{\mathrm{CH}}}(\omega) = (1/360)(\gamma_\mathrm{C}\gamma_\mathrm{H}\hbar\langle r_{\mathrm{CH}}^{-3}\rangle)^2[3(3\cos^2\beta - 1)^2\,\tau_{200}/(1 + (\omega\tau_{200})^2) + 36\cos^2\beta\sin^2\beta\tau_{210}/(1 + (\omega\tau_{210})^2) + 9\sin^4\beta\tau_{220}/(1 + (\omega\tau_{220})^2) + 48\sin^2\beta\cos^2\beta\tau_{201}/(1 + (\omega\tau_{201})^2) + 16(4\cos^4\beta - 3\cos^2\beta + 1)\tau_{211}/(1 + (\omega\tau_{211})^2) + 16\sin^2\beta(1 + \cos^2\beta)\tau_{221}/(1 + (\omega\tau_{221})^2) + 24\sin^4\beta\tau_{202}/(1 + (\omega\tau_{202})^2) + 32\sin^2\beta(1 + \cos^2\beta)\tau_{212}/(1 + (\omega\tau_{212})^2) + 8(\cos^4\beta + 6\cos^2\beta + 1)\tau_{222}/(1 + (\omega\tau_{222})^2)] \quad (9)$$

However, in the vicinity of the T_1 minimum, where $\tau_{2n0}/(1 + (\omega\tau_{2n0})^2) \gg \tau_{2nk\neq0}/(1 + (\omega\tau_{2nk\neq0})^2)$, rapid methyl motions project all interactions onto the common triad axis and the relevant dipole−dipole spectral densities tend toward the limiting values

$$J^{D_{\mathrm{CH}}}(\omega) = (1/120)\,(\gamma_\mathrm{C}\gamma_\mathrm{H}\hbar\langle r_{\mathrm{CH}}^{-3}\rangle)^2[(3\cos^2\beta - 1)^2\tau_{200}/(1 + (\omega\tau_{200})^2) + 12\cos^2\beta\sin^2\beta\tau_{210}/(1 + (\omega\tau_{210})^2) + 3\sin^4\beta\tau_{220}/(1 + (\omega\tau_{220})^2)] \quad (10a)$$

$$K^{D_{\mathrm{CH}}D_{\mathrm{CH}'}}(\omega) = J^{D_{\mathrm{CH}}}(\omega) \quad (10b)$$

$$J^{D_{\mathrm{HH}'}}(\omega) = (9/4)(\gamma_\mathrm{H}/\gamma_\mathrm{C})^2(\langle r_{\mathrm{HH}'}^{-3}\rangle/\langle r_{\mathrm{CH}}^{-3}\rangle)^2\,J^{D_{\mathrm{CH}}}(\omega) \quad (10c)$$

$$K^{D_{\mathrm{HH}'}D_{\mathrm{HH}''}}(\omega) = J^{D_{\mathrm{HH}'}}(\omega) \quad (10d)$$

$$K^{D_{\mathrm{CH}}D_{\mathrm{HH}'}}(\omega) = (3/2)(\gamma_\mathrm{H}/\gamma_\mathrm{C})\langle r_{\mathrm{HH}'}^{-3}\rangle/\langle r_{\mathrm{CH}}^{-3}\rangle\,J^{D_{\mathrm{CH}}}(\omega) \quad (10e)$$

$$Q^{D_{\mathrm{CH}}D_{\mathrm{CH}'}}(\omega) = (1/120)\,(\gamma_\mathrm{C}\gamma_\mathrm{H}\hbar\langle r_{\mathrm{CH}}^{-3}\rangle)^2(1/\omega)[(3\cos^2\beta - 1)^2/(1 + (\omega\tau_{200})^{-2}) + 12\cos^2\beta\sin^2\beta/(1 + (\omega\tau_{210})^{-2}) + 3\sin^4\beta/(1 + (\omega\tau_{220})^{-2})] \quad (10f)$$

$$Q^{D_{\mathrm{CH}}D_{\mathrm{HH}'}}(\omega) = (3/2)(\gamma_\mathrm{H}/\gamma_\mathrm{C})\langle r_{\mathrm{HH}'}^{-3}\rangle/\langle r_{\mathrm{CH}}^{-3}\rangle\,Q^{D_{\mathrm{CH}}D_{\mathrm{CH}'}} \quad (10g)$$

It is important to remember that eqs 10 are limiting values for more complicated expressions derivable from eqs 8. (Of course, the complete expressions, eqs 8, were used in our analysis.) If one inserts the known relations, $(\gamma_\mathrm{H}/\gamma_\mathrm{C}) = 3.98$ and $\langle r_{\mathrm{HH}'}^{-3}\rangle/\langle r_{\mathrm{CH}}^{-3}\rangle = (3/8)^{3/2}$, further simplifications result.

For a cylindrically symmetric ^{13}C shielding anisotropy (whether actual or assumed), the principal shielding axis is collinear with the triad axis. (Comments on the adequacy of the axial symmetry assumption will be given in the Discussion.) Thus, in the limit, $\tau_{2n0}/(1 + (\omega\tau_{2n0})^2) \gg \tau_{2nk\neq0}/(1 + (\omega\tau_{2nk\neq0})^2)$,

$$J^{\mathrm{SAC}}(\omega) = (1/120)\,(\Delta\sigma_\mathrm{C}\omega_\mathrm{C})^2[(3\cos^2\beta - 1)\tau_{200}/(1 + (\omega\tau_{200})^2) + 12\cos^2\beta\sin^2\beta\,\tau_{210}/(1 + (\omega\tau_{210})^2) + 3\sin^4\beta\tau_{220}/(1 + (\omega\tau_{220})^2)] \quad (11a)$$

$$K^{D_{\mathrm{CH}}\mathrm{SA_C}}(\omega) = -\{(\gamma_\mathrm{C}\gamma_\mathrm{H}\hbar\langle r_{\mathrm{CH}}^{-3}\rangle)/(\Delta\sigma_\mathrm{C}\omega_\mathrm{C})\}J^{\mathrm{SA_C}}(\omega) \quad (11b)$$

$$K^{D_{\mathrm{CH}}\mathrm{SA_H}}(\omega) = (-1/3)(\Delta\sigma_\mathrm{H}\omega_\mathrm{H}/\Delta\sigma_\mathrm{C}\omega_\mathrm{C})K^{D_{\mathrm{CH}}\mathrm{SA_C}}(\omega) \quad (11c)$$

$$Q^{D_{CH}SA_C}(\omega) = (-1/120)(\gamma_C\gamma_H\hbar\langle r_{CH}^{-3}\rangle)(\Delta\sigma_C\omega_C)(1/\omega) \times [(3\cos^2\beta - 1)/(1 + (\omega\tau_{200})^{-2}) + 12\cos^2\beta\sin^2\beta/(1 + (\omega\tau_{210})^{-2}) + 3\sin^4\beta/(1 + (\omega\tau_{220})^{-2})] \quad (11d)$$

The expression for $K^{D_{CH}SA_H}(\omega)$ assumes that the proton shielding anisotropy is cylindrically symmetric about the C−H bond. In the context of this study, this is a moot point.

V. Results

The temperature dependence of the carbon T_1 for a 0.85 M solution of methanol in glycerol-d_8 is displayed in Figure 1. The T_1 values (defined in eq 1a) were calculated from the initial slopes obtained from a proton (CW) decoupled carbon inversion−recovery experiment. The minimum in the T_1 curve occurs near 5 °C, and it is predicted that effects associated with the dynamic frequency shift will be most apparent in the vicinity of this temperature.

Figure 2 shows the normalized intensities of the quartet lines obtained in the (proton) hard pulse experiment at 5 °C. At this temperature, the nominal (^{13}C) T_1 is 1.05 s. It is apparent that the usual $5T_1$ delay between scans fails to allow the individual multiplet magnetizations to reach their full thermal equilibrium values which are reached only after a period equal to about $25T_1$'s. Due to the high degree of (cross) correlation, the differential responses of each line of the quartet immediately after the perturbation of the spin system are remarkable.

In Figure 3, different shifts for the components of the inner lines of the quartet are clearly visible. The clarity of this observation results from the opposite phase of the narrow and broad components of these inner lines. The narrow peak in Figure 3 (35 °C) appears at a lower frequency from the broad peak, in marked contrast to results at lower temperatures, e.g., Figure 4 (−5 °C), where the narrow peak again passes through its null point at a slower rate, but at higher frequency.

The automated analysis software 1D_ANALYSIS, discussed above, was used to analyze the methanol spectral data. The quartet lines were fit, assuming that the inner lines were superpositions of two Lorentzian lines. Because of the high correlation between the spectral parameters (frequency, line width, intensity, and phase), it was necessary to lock some of these parameters. First, the phase function for each series of spectra was adjusted then locked for the remainder of the analysis. Furthermore, an *averaged* line width of each component of the inner lines was determined in the d2 range where the other component is null or very weak, and then this parameter was locked. An example of this analysis is given in Figure 4 where the spectrum is decomposed into six lines. The success of this process is shown at the top of this figure with the very small residuals that are obtained when the component lines are subtracted from the experimental spectrum given at the bottom of the figure.

It should be stressed that this analysis assumes that the inner lines of the quartet have only two components.[47] For d2 ranges where the two components have opposite phases, it is possible to unlock the frequencies and the line widths in the analysis, and under these conditions only very slight variations in these frequencies and line widths are observed. An extremely good fit of the experimental line shapes of the inner lines of the quartet was obtained with the assumption of only two Lorentzians. Although theory permits more complicated superpositions, the use of additional components was not felt to be justified. Thus, the carbon quartet in $^{13}CH_3OD$ was simulated by six Lorentzians. To be consistent in all experiments, only the intensity and

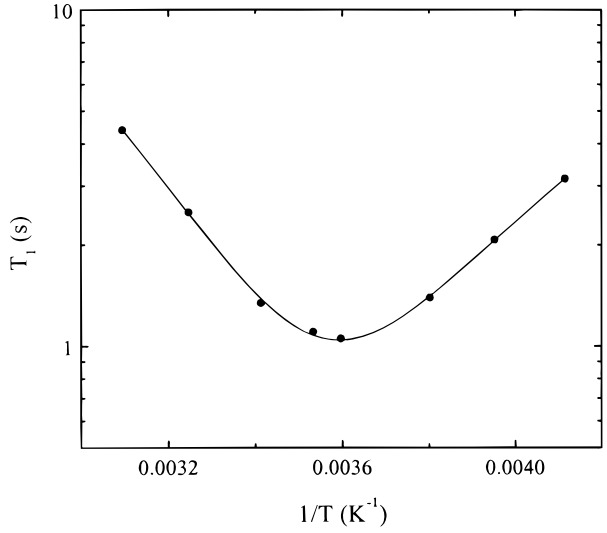

Figure 1. Variation of the carbon T_1 values (obtained from proton decoupled carbon inversion−recovery experiments) versus $1/T$. Spectra were obtained at 9.4 T.

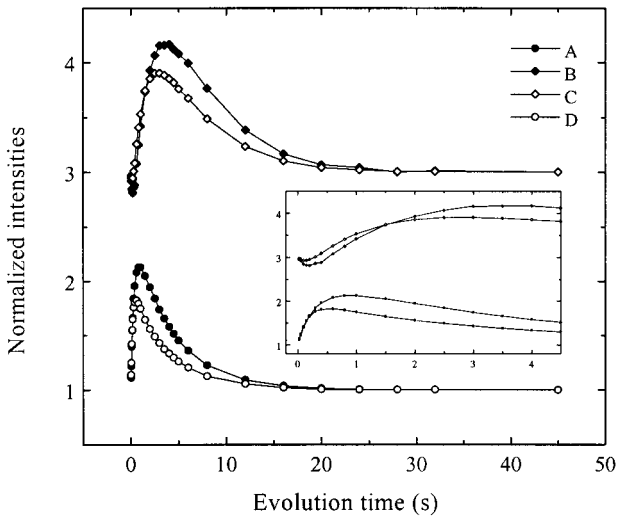

Figure 2. Individual ^{13}C multiplet responses after the perturbation effected by inversion of proton magnetization. Lines A, B, C, and D are the ^{13}C quartet components, from high frequency to low frequency. Spectra were obtained at 11.7 T at a temperature of 5 °C.

frequency parameters were ultimately unlocked in the final spectral analysis. These simulations were used to evaluate both the magnetization modes and the frequencies of all the components of the quartet. Additional Lorentzians were also used to account for the small amount (∼5%) of $^{13}CH_3OH$ in the labeled sample.

The real parts of three dipole−dipole spectral densities and one dipole-shielding anisotropy spectral density were evaluated from the initial responses of various magnetization modes after carbon inversion and proton inversion perturbations at 11.7 T. The values of these parameters are given in Table 1. Using a standard tetrahedral geometry, plots of J (or K) as a function of $D_{||}$ were generated for different values of D_i and β. Considering only the dipole−dipole spectral densities (see Discussion), the best sets of ($D_\perp$, $D_{||}$) values were obtained for $D_i = 2 \times 10^{12}$ rad/s and $\beta = 90°$ and are also included in Table 1. In contrast to the values of the spectral densities, the errors given for the diffusion constants are not standard deviations but reflect the ranges of values of these constants needed to make them coherent with the ranges of the experimental values of the three spectral densities. The variations of the diffusion constants

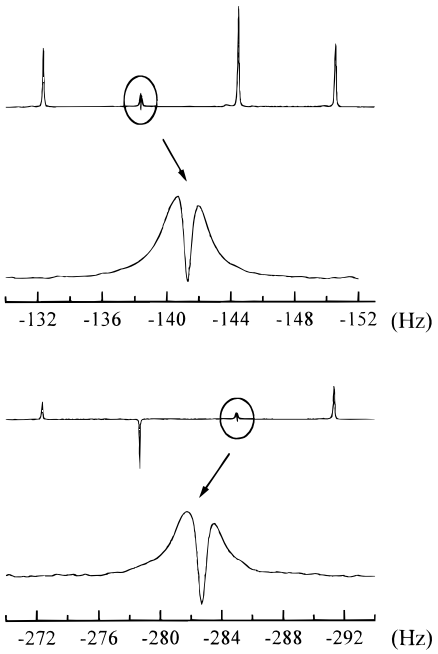

Figure 3. Carbon inversion−recovery (CIR) experiment. Evolution time: 3.0 s (top); 1.6 s (bottom). Spectra were obtained at 11.7 T at a temperature of 35 °C.

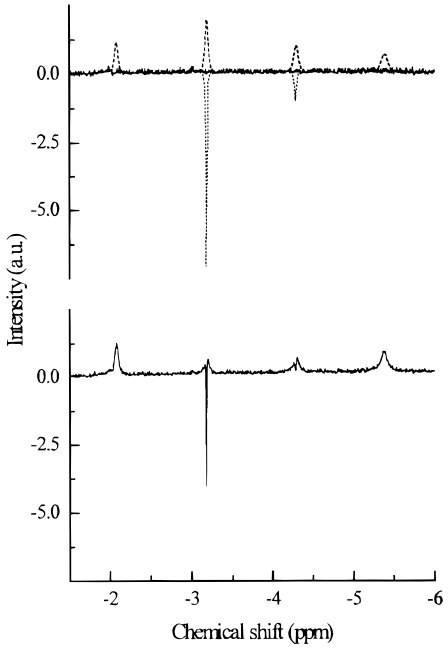

Figure 4. Analysis of a carbon-inversion recovery spectrum (evolution time 1.6 s) by the program 1D_ANALYSIS. Top: components lines and residuals; bottom: experimental spectrum at 11.7 T and −10 °C.

versus $1/T$ are shown in Figure 5. In these Arrhenius-type plots, the apparent activation energy associated with $D_\perp$ is 49 ± 4 kJ/mol.

The temperature dependence of the spectral densities, $K^{D_{CH}D_{CH'}}(\omega_C)$, $K^{D_{CH}D_{HH'}}(\omega_H)$, $K^{D_{CH}SA_C}(\omega_C)$, and the combination, $2J^{D_{CH}}(\omega_C + \omega_H) - (1/3)J^{D_{CH}}(\omega_C - \omega_H)$, are displayed in Figure 6. The lines running through these experimental results were calculated using the values of the diffusion constants obtained from the linear fits of $\log(D)$ versus $1/T$, and $\Delta\sigma = 71$ ppm.[48]

The values of the imaginary parts of the spectral densities were calculated, at 11.7 T, from eqs 5 and 7 using the best set of motional parameters established by the real parts of the dipole−dipole spectral densities (see Table 1). These values are given in Table 2.

The differential dynamic frequency shifts, $\Delta(\delta\nu)$, calculated from equations 4 and 6 are given in Table 3 along with the experimental values of the differences of frequencies of the corresponding lines (line A is the highest frequency component and line D is the lowest frequency component). The $\nu_A - \nu_D$ values are the average of all the carbon inversion−recovery data. This analysis requires the use of the high-temperature splitting as a fiducial value to extract from $\nu_A - \nu_D$ the value of $3J_{CH}$. The values given for $(\nu_{broad} - \nu_{narrow})$ for the central lines (B and C) were determined from the (CIR) spectra where the broad and narrow components have clearly opposite phases. It is obvious that the observed shifts appear to be substantially larger than the dynamic frequencies predicted by theory. Some suggestions for this discrepancy are given in the following section.

VI. Discussion

The internal motion of the methyl group about the triad axis is very rapid, and hence, even the dipolar (cross-correlation) spectral densities are insensitive to this motion. The data can only provide a reliable lower limit, $D_i \approx 10^{12}$ rad/s and, for simplicity, in all subsequent analyses, it is assumed that $D_i = 2 \times 10^{12}$ rad/s. In contrast, the dipolar spectral densities are very sensitive to the value of β. The three dipole−dipole spectral densities measured are interpretable only if $\beta = 90 \pm 5°$. For any other value of β, no set of $(D_\perp, D_\parallel)$ values "explain" the data. This result rules out the "internal rotator attached to an isotropic tumbler" model often used for the reorientational dynamics of methanol. A model assuming rapid exchange between two different environments, as suggested in a recent paper,[49] was unsuccessful in rationalizing the experimental data.

In a binary solution of alcohols, it is expected that hydrogen bonding plays an important role, and the existence of polymeric chains of methanol/glycerol is consistent with the motional anisotropy that strongly increases with decreasing temperatures. This model is consistent with $\beta = 90°$ (see Figure 7). The fact that $D_\parallel$ depends only slightly upon temperature is somewhat surprising. However, when $\beta = 90°$, the strong dependence of the real parts of the dipolar spectral densities on $D_\parallel$ renders this result unambiguous. Likewise, the good agreement between the experimental and calculated spectral densities obtained from the CIR experiments at 9.4 T (see Table 4) confirms that these values are correct. The high value for the apparent activation energy for $D_\perp$ is less than the corresponding value (58 ± 2 kJ/mol) that can be calculated from the variation of the correlation time of neat perdeuterated glycerol versus temperature[16] (glycerol was modeled as a rigid spherical top, and its diffusion constant was determined as 2.6 (±0.7) × 10^7 rad/s at 5 °C, what is about 7 times smaller than the Dperp value of methanol at the same temperature).

The noticeable differences between the relaxation rates of lines A and D, and between those of lines B and C, indicate significant two-spin order induced by relaxation (see Figures 2−4). Also, this is evidenced by the differential broadenings of the outermost members of the quartet (see Figure 4). However, only the three dipole−dipole spectral densities have been used to estimate the dynamics of methanol. This is because eqs 2b and 2d, which assume a symmetrical chemical shielding tensor with its principal axis along the triad axis, predict values moderately inconsistent with experiment (see Figure 6).

It is recognized that the orientation of the carbon shielding tensor in methanol is not known a priori since the C_3 symmetry

TABLE 1: Values of the Real Parts of the Spectral Densities Obtained from the Initial Slopes of Some Magnetization Modes and Values of the Diffusion Constants Obtained by a Graphical Resolution of the Expressions $J(\omega)$ (or $K(\omega)$) = $f(D_\perp, D_{||}, D_i,\beta,\omega)$ Related to the Dipole−Dipole Spectral Densities[c]

T (°C)	$f[J^{D_{CH}}(\omega)]$[a] $\times 10^2$ (rad/s)	$K^{D_{CH}D_{CH'}}(\omega_C)$ $\times 10^2$ (rad/s)	$K^{D_{CH}D_{HH'}}(\omega_H)$ $\times 10^2$ (rad/s)	$K^{D_{CH}SA_C}(\omega_C)$ $\times 10^2$ (rad/s)	$D_\perp \times 10^{-8}$ (rad/s)	$D_{||} \times 10^{-10}$ (rad/s)
35	4.7(1)	3.8(4)	4.7(1)	−1.7(2)	8(1)	1.7(3)
5	3.1(1)	13(2)	4.3(1)	−6.5(9)	2.0(4)	1.3(3)
−10[b]		7(1)		−3.9(6)	0.4(1)	1.0−2.0
−20	1.8(1)	2.9(3)	1.2(3)		0.12(2)	1.4(2)

[a] Only the combination $f[J^{D_{CH}}(\omega)] = 2J^{D_{CH}}(\omega_H + \omega_C) - (1/3)J^{D_{CH}}(\omega_H - \omega_C)$ can be evaluated from the initial slope of the $^a\nu_1$ magnetization mode of the hard pulse experiment. [b] At this temperature, only the carbon-inversion recovery experiment has been done, yielding one dipole−dipole spectral density. Therefore, the range of $D_{||}$ values has been chosen as to cover all the values obtained at the other temperatures, allowing the evaluation of the maximum range of $D_\perp$ values from the graph $K^{D_{CH}D_{CH'}}(\omega_C) = f(D_\perp,D_{||},D_i,\beta,\omega_C)$. [c] D_i was locked to 2×10^{12} rd/s and β to 90° (see text); 11.7 T.

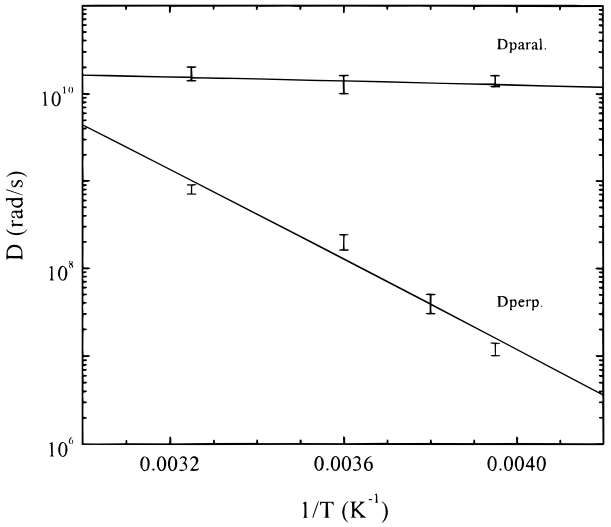

Figure 5. Variations of the diffusion constants versus $1/T$. $D_{internal}$ and β were locked to 2×10^{12} rad/s and 90°, respectively (see text).

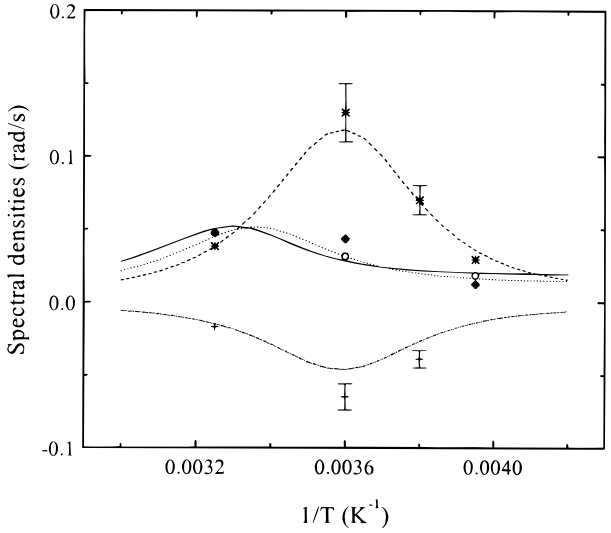

Figure 6. Variations of the real parts of the spectral densities versus $1/T$. The curves were calculated with the values of the diffusion constants obtained from the linear fits of $\log(D)$ versus $(1/T)$, and $\Delta\sigma$ = 71 ppm: solid line and open circles, $f[J^{D_{CH}}(\omega)]$; dashed line and stars, $K^{D_{CH}D_{CH'}}(\omega_C)$; dotted line and diamonds, $K^{D_{CH}D_{HH'}}(\omega_H)$; dotted dashed line and crosses, $K^{D_{CH}SA_C}(\omega_C)$. The data were taken at 11.7 T.

is slightly broken by the OH group. However, in the presence of rapid motion about the triad axis, effects due to asymmetry in the shielding tensor are effectively eliminated. Furthermore, modest angular deviations[51] between the principal axis of the shielding tensor and the CO axis (<10°) result in no appreciable

TABLE 2: Values of the Imaginary Parts of the Spectral Densities[a] Calculated at 11.7 T from the Values of the Diffusion Constants, with $\Delta\sigma$ = 71 ppm

T (°C)	$Q^{D_{CH}D_{CH'}}(\omega_H - \omega_C)$ $\times 10^2$ (rad/s)	$Q^{D_{CH}D_{CH'}}(\omega_H + \omega_C)$ $\times 10^2$ (rad/s)	$Q^{D_{CH}D_{HH'}}(\omega_H)$ $\times 10^2$ (rad/s)	$Q^{D_{CH}SA_C}(\omega_C)$ $\times 10^2$ (rad/s)
35	1.5(3)	1.9(3)	2.4(3)	−0.24(8)
5	5.9(4)	4.1(1)	6.7(3)	−2.7(8)
−10	7.34(4)	4.50(2)	7.65(5)	−7.7(3)
−20	7.40	4.52	7.68	−8.44(5)

[a] The figures in parentheses are the errors propagated from the errors on $D_\perp$.

modifications of eq 11b or its more general counterpart, eq 8a. Thus, the assumption of axial symmetry is perfectly valid. However, it is interesting to note that the apparent shielding anisotropy is somewhat larger than commonly accepted.[48,50]

As stated in the Results, the shift data cannot be explained, completely, by the proposed theory. At 35 °C, the differences between the frequencies of the components of the inner lines have a sign opposite to the calculated one. Furthermore, at lower temperatures, these differences are much larger than the $\Delta(\delta\nu)$ values predicted by theory (see Table 3). It should be noted that if and only if the coupling between the proton quartet and doublet states is zero are the inner lines of the quartet rigorously described as two Lorentzians with a broad line and a narrow line (corresponding to the quartet and doublet states, respectively) with well defined differential shifts. However, the very small residuals obtained by such an analysis of our data (see Figure 4) indicate that the influence of this coupling is negligible as a first approximation.

These observations suggest that additional mechanisms, still unidentified and thus not taken into account in our theoretical models, may be responsible for small frequency shifts near the T_1 minimum. In addition to the dynamic frequency shift, at high magnetic field strengths, one may expect small shifts associated with induced molecular alignment.[51] Such a mechanism could induce a weak temperature dependence of the scalar coupling constant in addition to the very small intrinsic[52] temperature dependence of this coupling constant. However, either of these temperature effects would influence the frequency of the six lines of the quartet identically. Therefore, they cannot explain the observed variations of the splitting of the central quartet components versus temperature.

It is interesting to note a few characteristics of the unusual features observed for the methanol spectra. First, they do not depend on the perturbation of the spin system. Similar values for $(\nu_{broad} - \nu_{narrow})_{B,C}$ are obtained when line B or C goes through a null intensity in soft-pulse and J-pulse experiments.[26] The sign of $(\nu_{broad} - \nu_{narrow})_{B,C}$ is the same for the CIR spectra obtained at 9.4 and 11.7 T on the same methanol/glycerol solution. The analysis of the CIR data obtained at 11.7 T shows

TABLE 3: Comparison of the Differences between the Experimental Frequencies of the Components of the Carbon Lines[a] of Methanol with the Differences $\Delta(\delta\nu)$ between the Dynamic Frequency Shifts Calculated at 11.7 T

T (°C)	$\nu_A - \nu_D$ (Hz)	$\Delta(\delta\nu)$ (Hz)	$(\nu_b - \nu_n)_B$ (Hz)	$(\nu_b - \nu_n)_C$ (Hz)	$\Delta(\delta\nu)$ (Hz)	$(\nu_B - \nu_C)_b$ (Hz)	$(\nu_B - \nu_C)_n$ (Hz)	$\Delta(\delta\nu)$ (Hz)
35[b]	0.00	−0.005(2)	0.03(1)	0.08(1)	−0.007(3)	−0.03(1)	0.02(2)	−0.002
5	−0.13(2)	−0.05(2)	−0.06(1)	0.00(3)	−0.034(5)	−0.11(3)	−0.04(2)	−0.017(5)
−10	−0.14(3)	−0.147(6)	−0.23(2)	−0.6(1)	−0.042(1)	0.30(7)	−0.06(3)	−0.049(2)
−20	−0.93(3)	−0.161(1)	−1.1(2)	−0.9(1)	−0.042	−0.32(16)	−0.14(12)	−0.054

[a] The subscripts "b" and "n" represent the broad and narrow components, respectively, of the inner lines B and C of the quartet. [b] The $\nu_A - \nu_D$ experimental values are referenced to the value 424.10(1) Hz ($\equiv 3\,J_{CH}$) observed at 35 °C. The $(\nu_B - \nu_C)_b$ and $(\nu_B - \nu_C)_n$ experimental values are referenced to J_{CH}.

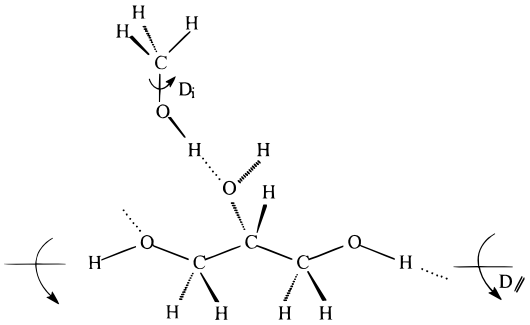

Figure 7. A simple structure for methanol hydrogen bonded to polymeric glycerol.

TABLE 4: Comparison of the Experimental Values[a] of the Real Parts of the Spectral Densities Obtained at 9.4 T with the Values Calculated with the Same Set of Parameters as in Figure 6

	$K^{D_{CH}D_{CH'}}(\omega_C) \times 10^2$ (rad/s)		$K^{D_{CH}SA_C}(\omega_C) \times 10^2$ (rad/s)	
T (°C)	exptl	calcd	exptl	calcd
35	4.1(1)	3.8	−1.5(2)	−1.2
5	18(2)	14	−5.9(6)	−4.5
−20	4.2(3)	5.0		

[a] The numbers in parentheses are the standard deviations in units of the last digits.

that $(\nu_B - \nu_C)_{narrow}$ decreases only very slightly with temperature, as required by the theory which predicts $(\nu_B - \nu_C)_{n,b}$ to be equal to $J_{CH} + 4\{Q^{D_{CH}SA_C}(\omega_C) + Q^{D_{CH}SA_H}(\omega_H)\}/2\pi$, but $(\nu_B - \nu_C)_{broad}$ behaves erratically (see Table 3). This same behavior of the narrow and broad components of the inner lines of a quartet has been observed for *m*-cresol in a gel.[53] Therefore, it seems that the frequencies of the broad lines, associated with the proton quartet states, are influenced by some unknown phenomena(on) which mask(s) the dynamic frequency shifts. Investigation of these anomalies is in progress.

It should be mentioned that only a small fraction of the methanol/glycerol relaxation data gathered has been presented. All of the data obtained at 11.7 T are given in the Supporting Information. It is acknowledged that the graphical approach used in this paper yields only an estimation of the dynamics of molecules. The complexities of the problem and limitations of the theoretical model presently do not justify a complete fit of all the relaxation data needed to ascertain the precise values of all the motional parameters.

VII. Conclusions

Few detailed nuclear spin relaxation studies have been designed outside the extreme narrowing limit. Many experimental difficulties are involved in relaxation studies of viscous solutions. As the deuterium resonances of the solvent (glycerol) are too broad for ultrahigh-precision locking, a new software, LOCKIT, was developed to alleviate this problem.

The present study of methanol in glycerol makes use of the cross-correlated spectral densities which are increasingly[54] utilized to differentiate among various models of molecular motions. The values of the real parts of three dipole−dipole spectral densities were obtained from the initial response of various magnetization modes in carbon inversion−recovery and hard pulse experiments. A free rotator attached to a symmetric top diffuser was the simplest motional model that could explain the data. The methyl group rotates about an axis perpendicular to the principal axis of this symmetric top. This model is consistent with a strongly associated, hydrogen-bonded methanol/glycerol solution-state structure.

The relatively simple methodologies described in this work yield valuable information on the dynamics of methanol, and such an approach promises to provide valuable insights on the dynamics of biopolymers, using carbon-13 enriched methyl groups as a local probe. The methyl group is uniquely positioned to monitor site-specific dynamics because (i) there are numerous relaxation pathways available for this four-spin system and (ii) the rapid internal motion effectively renders all competing interactions completely correlated, hence maximizing various relaxation-induced polarization transfer pathways.

Finally, this study clearly demonstrates that the two inner lines of the quartet have at least two components with clearly different relaxation rates and frequencies. However, the magnitudes of the relaxation-induced shifts of the various components lack consistency with theory, and carefully designed experiments and/or improved theoretical models are needed to clarify this matter. Such a study is in progress.

Appendix

For the AX_n spin system where spin A (associated with the angular momentum $I = 1/2$) and n magnetically equivalents spins X (associated with angular momenta $S^{(1)}$, $S^{(2)}$,..., $S^{(n)} = 1/2$) are relaxed by anisotropic shieldings and mutual dipolar interactions, application of standard methods[11] can be used to derive the relevant second order dynamic frequency shifts for all coherences in this system. It is assumed that the X spins are magnetically equivalent. Of course, any frequency shift can be described equivalently by invoking a redefined time-averaged Hamiltonian.[55] When applied to the present problem, the redefined H_o (in s^{-1}) assumes the form

$$H_o/\hbar = -(\omega_A + \rho_A)\{I_z\} - (\omega_X + \rho_X)\sum_i S_z^{(i)} + 2\pi J_{AX}\{I_z\sum_i S_z^{(i)}\} + 2\pi J_{XX'}\{\sum_{i<j} S^{(i)}S^{(j)}\} + 4\delta_{AX}\{I_z\sum_i S_z^{(i)}\} + 4\delta_{XX'}\{\sum_{i<j} 3S_z^{(i)}S_z^{(j)} - S^{(i)}S^{(j)}\} - 4\mu\{I_z(\sum_{i<j} S_z^{(i)}S_z^{(j)})\} - \rho_{XAX'}\{I_z\sum_{i\neq j} S_+^{(i)}S_-^{(j)}\} - 12\lambda_{XX'X''}\{\sum_{i<j<k} S_z^{(i)}S_z^{(j)}S_z^{(k)}\} + 2\rho_{XX'X''}\{\sum_{i<j\neq k} S_z^{(i)}S_+^{(j)}S_-^{(k)}\} \quad \text{(A1)}$$

where

$$\rho_A = n\{(1/6)Q^{D_{AX}}(\omega_A - \omega_X) + (1/2)Q^{D_{AX}}(\omega_A) + Q^{D_{AX}}(\omega_A + \omega_X)\} + 2Q^{SA_A}(\omega_A)$$

$$\rho_X = (1/6)Q^{D_{AX}}(\omega_X - \omega_A) + (1/2)Q^{D_{AX}}(\omega_X) + Q^{D_{AX}}(\omega_A + \omega_X) + 2Q^{S_{AX}}(\omega_X) + (n-1)\{(1/2)Q^{D_{XX'}}(\omega_X) + Q^{D_{XX'}}(2\omega_X)\}$$

$$\rho_{XX'X''} = Q^{D_{XX'}D_{XX''}}(\omega_X) + Q^{D_{XX'}D_{XX''}}(2\omega_X)$$

$$\lambda_{XX'X''} = Q^{D_{XX'}D_{XX''}}(\omega_X)$$

$$\delta_{AX} = Q^{D_{AX}SA_A}(\omega_A) + Q^{D_{AX}SA_X}(\omega_X)$$

$$\delta_{XX'} = Q^{D_{XX'}SA_X}(\omega_X)$$

$$\mu = Q^{D_{AX}D_{AX'}}(\omega_A) + 2Q^{D_{AX}D_{XX'}}(\omega_X)$$

$$\rho_{XAX'} = (1/3)Q^{D_{AX}D_{AX'}}(\omega_A - \omega_X) - 2Q^{D_{AX}D_{XX'}}(\omega_X) + 2Q^{D_{AX}D_{AX'}}(\omega_A + \omega_X)$$

The terms $Q^{\eta\eta'}$ were defined previously in eqs 5 and 7. With this redefined isotropic Hamiltonian, all imaginary contributions to the spectral density can be simply ignored. Equation A1 is valid for the description of any AX_n spin-1/2 system for $n \geq 1$.

This equation renders apparent numerous features. Autocorrelated, imaginary spectral density contributions (Q's identified by a single superscript) do not differentiate between various spectral components and, hence, result in a very small overall multiplet displacement. Conversely, frequency shifts arising from cross-correlated processes do not displace a multiplet's weighted average frequency. Equivalently, eq A1 reaffirms that cross-correlated dynamic frequency shifts are intimately associated with relaxation-induced coherence transfers.[7] Dipole−dipole interference induces coherence transfer between spin order of similar parity whereas dipole-shielding anisotropy induces coherence transfer between spin orders of opposite parity with respect to spin inversion.[56]

The specific frequencies associated with the six unique single-quantum spin A transitions in the AX_3 spin system are

$$\langle\beta A_{\pm3/2}| \leftrightarrow \langle\alpha A_{\pm3/2}|; \quad \omega_A \mp 3/2(2\pi J_{AX} + 4\delta_{AX}) + 3\mu + \rho_A$$

$$\langle\beta A_{\pm1/2}| \leftrightarrow \langle\alpha A_{\pm1/2}|; \quad \omega_A \mp 1/2(2\pi J_{AX} + 4\delta_{AX}) - \mu + 2\rho_{XAX'} + \rho_A$$

$$\langle\beta E_{\pm1/2}| \leftrightarrow \langle\alpha E_{\pm1/2}|; \quad \omega_A \mp 1/2(2\pi J_{AX} + 4\delta_{AX}) - \mu - \rho_{XAX'} + \rho_A \quad \text{(A2)}$$

Thus, within the ^{13}C quartet, it is easily seen that splitting, in Hz, between the outermost lines $\langle\beta A_{-3/2}|H_o/h|\beta A_{-3/2}\rangle - \langle\alpha A_{-3/2}|H_o/h|\alpha A_{-3/2}\rangle - \langle\beta A_{+3/2}|H_o/h|\beta A_{+3/2}\rangle + \langle\alpha A_{+3/2}|H_o/h|\alpha A_{+3/2}\rangle$, is given by $3J_{AX} + 12\delta_{AX}/2\pi$ and, in the absence of dipole−dipole cross-correlation, the splitting between the two central transitions is given by $J_{AX} + 4\delta_{AX}/2\pi$. Similarly, if dipole−dipole interference dominates, the degeneracy of the central transitions is partially lifted and the resulting differential shift, $\langle\beta A_{\pm1/2}|H_o/h|\beta A_{\pm1/2}\rangle - \langle\alpha A_{\pm1/2}|H_o/h|\alpha A_{\pm1/2}\rangle - \langle\beta E_{\pm1/2}|H_o/h|\beta E_{\pm1/2}\rangle + \langle\alpha E_{\pm1/2}|H_o/h|\alpha E_{\pm1/2}\rangle$, equals $3\rho_{XAX'}/2\pi$. In the preceding discussion, the abbreviations α and β are used for $m_I = +1/2$ and $m_I = -1/2$, respectively, and standard notations are employed as labels for the quartet ($A_{\pm3/2}$, $A_{\pm1/2}$), doubly degenerate doublet ($E_{\pm1/2}$), spins-X.

In NMR, absolute signs are a source of continual confusion[57] and nowhere is this more evident than in discussions related to cross-correlated dynamic frequency shifts where $Q^{\eta\eta'}(\omega) = -Q\eta\eta'(-\omega)$. The present definition states that for positive J_{AX}, γ_A, γ_X, $\Delta\sigma_A$ and positive correlation factor, $(1/2)(3\cos^2\Theta_{D_{AX}SA_{(X)}}-1)$ for isotropic motions, dipole-shielding anisotropy cross correlation shifts the $\beta \leftrightarrow \alpha$ ($m_s = A_{+3/2}$) coherence to lower frequency and the $\beta \leftrightarrow \alpha$ ($m_s = A_{-3/2}$) coherence to higher frequency thus increasing the apparent spectral width of the multiplet. Likewise, for positive J_{AX}, γ_A, γ_X, and positive correlation factors, dipole−dipole interference shifts the $\beta \leftrightarrow \alpha$ ($m_s = A_{\pm3/2}$) coherences to higher frequencies. In this situation, the separation between the two lower frequency components is less than the separation between the two higher frequency components.

Supporting Information Available: Carbon relaxation data obtained on methanol $^{13}CH_3OD$ (0.85 M in glycerol-d_8), after different perturbations of either the proton or carbon magnetization (Varian spectrometer VXR-500, 11.7 T). This material is available free of charge via the Internet at http://pubs.acs.org.

References and Notes

(1) Cavanagh, J.; Fairbrother, W. J.; Palmer, A. G.; Skelton, N. J. *Protein NMR Spectroscopy*; Academic Press: New York, 1996.

(2) Dayle, K. T.; Wagner, G.; Lefevre, J. F. *Annu. Rev. Phys. Chem.* **1996**, *47*, 243.

(3) Liu, F.; Horton, W. J.; Mayne, C. L.; Xiang T.; Grant, D. M. *J. Am. Chem. Soc.* **1992**, *114*, 5281.

(4) Werbelow, L. G.; Grant, D. M. *J. Chem. Phys*. **1975**, *63*, 544.

(5) Werbelow, L. G.; Grant, D. M. *Adv. Magn. Reson*. **1977**, *9*, 189.

(6) Grant, D. M.; Mayne, C. L.; Liu, F.; Xiang, T. X. *Chem. Rev*. **1991**, *91*, 1591.

(7) Werbelow, L. G. In *Nuclear Magnetic Probes of Molecular Dynamics*; Tycko, R., Ed.; Kluwer: Norwell, MA, 1994; p 223.

(8) Redfield, A. G. *IBM J. Res. Develop*. **1957**, *1*, 19; *Adv. Magn. Reson*. **1965**, *1*, 1.

(9) Grant, D. M.; Brown, R. A. In *Encyclopedia of Nuclear Magnetic Resonance*; Grant, D. M., Harris, R. K., Eds.; Wiley: London, **1996**, *6*, 4003.

(10) Fuson, M. M. In *Encyclopedia of Nuclear Magnetic Resonance*; Grant, D. M., Harris, R. K., Eds.; Wiley: London, **1996**, *3*, 1466.

(11) Werbelow, L. G. In *Encyclopedia of Nuclear Magnetic Resonance*; Grant, D. M., Harris, R. K., Eds.; Wiley: London, **1996**, *3*, 1776.

(12) Werbelow, L. G. In *Encyclopedia of Nuclear Magnetic Resonance*; Grant, D. M., Harris, R. K., Eds.; Wiley: London, **1996**, *6*, 4092.

(13) Werbelow, L. G.; London, R. E. *Concepts Magn. Reson*. **1996**, *8*, 325.

(14) Werbelow, L. G.; London, R. E. *J. Chem. Phys*. **1995**, *102*, 5181.

(15) London, R. E.; Le Master, D. M.; Werbelow, L. G. *J. Am. Chem. Soc.* **1994**, *116*, 8400.

(16) Grzesiek, S.; Bax, A. *J. Am. Chem. Soc*. **1994**, *116*, 10196.

(17) Murali, N.; Nageswara Rao, B. D. *J. Magn. Reson. A* **1996**, *118*, 202.

(18) Tjandra, N.; Grzesiek, S.; Bax, A. *J. Am. Chem. Soc.* **1996**, *118*, 6264.

(19) Brüschweiler, R. *J. Chem. Phys.* **1996**, *105*, 6164; *Chem. Phys. Lett*. **1996,** *257*, 119.

(20) Thevand, A.; Werbelow, L. G. *J. Magn. Reson*. **1992**, *97*, 192.

(21) Haslinger, E.; Lynden-Bell, R. M. *J. Magn. Reson*. **1978**, *31*, 33. Figure 1 shows spectra with an inverted narrow component and a positive broad one with slightly different frequencies.

(22) Haslinger, E.; Robien, W. *J. Am. Chem. Soc*. **1980**, *102*, 1237. Figure 1 shows clearly that the frequency difference between the narrow and broad components varies with the evolution time.

(23) Lee, T. S.; Hwang, L. P. *J. Magn. Reson*. **1990**, *89*, 51. Figure 2 shows spectra with an inverted narrow component and a positive broad one with slightly different frequencies.

(24) Werbelow, L. G.; Thevand, A.; Pouzard, G. *J. Chem. Soc., Faraday Trans. 2* **1979**, *75*, 971.

(25) Chenon, M. Th.; Dunkel, R.; Mayne, C. L.; Grant, D. M. 34th ENC, Saint-Louis, MO, 1993.

(26) Liu, F.; Mayne, C. L.; Grant, D. M. *J. Magn. Reson*. **1989**, *84*, 344.

(27) The program 1D_ANALYSIS is commercially available as part of the FRED (Full Reduction of Entire Datasets) multidimensional spectral

analysis package. The software is marketed by Varian Associates, Inc. The 1D__ANALYSIS program can analyze Chemagnetics, Bruker Aspect, Felix, and Varian FIDs as well as Varian VNMR spectra. The FRED software is supported on Intel-based Microsoft Windows NT 4.0 PCs and on UNIX workstations from IBM, Silicon Graphics, and Sun Microsystems. Depending on the capacity of the computer as well as spectral resolution and complexity, the numerical analysis of a 1D spectrum takes between seconds and a few minutes.

(28) Dunkel, R. Ph.D. Thesis, University of Utah, 1990.

(29) Dunkel, R.; Mayne, C. L.; Pugmire, R. J.; Grant, D. M. *Anal. Chem.* **1992**, *64*, 3133, 3150.

(30) Orendt, A. M.; Dunkel, R.; Horton, W. J.; Pugmire, R. J.; Grant, D. M. *Magn. Reson. Chem.* **1995**, *33*, 803.

(31) Harper, J. K.; Dunkel, R.; Wood, S. G.; Owen, N. L.; Li, D.; Cates, R. G.; Grant, D. M. *J. Chem. Soc., Perkin Trans.* **1996**, *2*, 91.

(32) Dunkel, R. Method for Correcting Spectral and Imaging Data and for Using such Corrected Data in Magnet Shimming. U.S. Patent 5,218,299, June 8, 1993.

(33) LeMaster, D. M.; Richards, F. M. *Biochemistry* **1988**, *27*, 142.

(34) Grzesiek, S.; Anglister, J.; Ren, H.; Bax, A. *J. Am. Chem. Soc*. **1993**, *115*, 4369.

(35) Yamazaki, T.; Lee, W.; Revington, M.; Mattiello, D. L.; Dahlquist, F. W.; Arrowsmith, C. H.; Kay, L. E. *J. Am. Chem. Soc*. **1994**, *116*, 6464.

(36) Farmer, B. T.; Venters, R. A. *J. Am. Chem. Soc*. **1995**, *117*, 4187.

(37) Olson, D. L.; Peck, T. L.; Webb, A. G.; Magin, R. L.; Sweedler, J. V. *Science* **1995**, *270*, 1967.

(38) Barbara, T. M. *J. Magn. Reson. A* **1994**, *109*, 265.

(39) Shaw, D. *Fourier Transform N.M.R. Spectroscopy*, 2nd ed.; Elsevier: Amsterdam, 1984; Chapter 6.

(40) Dunkel, R. Correction and Automated Analysis of Spectral and Imaging Data. U.S. Patent 5,572,125, November 5, 1996.

(41) Bain, D.; Lynden-Bell, R. M. *Mol. Phys*. **1975**, *30*, 325.

(42) Werbelow, L. G.; Grant, D. M.; Black, E. P.; Courtieu, J. M. *J. Chem. Phys*. **1978**, *69*, 2407.

(43) Hubbard, P. S. *J. Chem. Phys.* **1969**, *51*, 1647.

(44) Werbelow, L. G.; Marshall, A. G. *J. Magn. Reson*. **1973**, *11*, 299.

(45) Brink, D. M.; Satchler, G. R. *Angular Momentum*; Clarendon Press: Oxford, 1968.

(46) Shirota, H.; Pal, H.; Tominaga, K.; Yoshihara, K. *J. Phys. Chem.* **1996**, *100*, 14575.

(47) Smith, S. Private communication. Simulations of this AX_3 spin system by GAMMA indicate that the inner lines are composed of one broad line and four narrow lines with slightly different frequencies and T_2 values. This result suggests that differential T_1 values could exist which may introduce errors of unknown magnitude into our analysis.

(48) Solum, M. S.; Facelli, J. C.; Michl, J.; Grant, D. M. *J. Am. Chem. Soc*. **1986**, *108*, 6464.

(49) Lienin, S. F.; Brûschweiler, R.; Ernst, R. R. *J. Magn. Reson*. **1998**, *131*, 184.

(50) Robyr, P.; Meier, B. H.; Fischer, P.; Ernst, R. R. *J. Am. Chem. Soc*. **1994**, *116*, 5315.

(51) Tjandra, N.; Bax, A. *J. Magn. Reson*. **1997**, *124*, 512.

(52) Bennett, B.; Raynes, W. T.; Anderson, C. W. *Spectrochim. Acta* **1989**, *45A*, 821.

(53) Chenon, M. Th. Unpublished data, 1997.

(54) Daragan, V. A.; Mayo, K. H. *Prog. Nucl. Magn. Reson. Spectros.* **1997**, *31*, 63.

(55) Freed, J. H.; Fraenkel, G. K. *J. Chem. Phys*. **1963**, *39*, 326.

(56) Werbelow, L. G.; Thevand, A.; Pouzard, G. *J. Chim. Phys*. **1979**, *76*, 722.

(57) Levitt, M. H. *J. Magn. Reson*. **1997**, *126*, 164.